Case Studies in Thermal Engineering 23 (2021) 100814

Contents lists available at ScienceDirect

Case Studies in Thermal Engineering

journal homepage: http://www.elsevier.com/locate/csite

Ablation behavior studies of charring materials with different thickness and heat flux intensity

Jie Xiao [a], Oisik Das [b], Rhoda Afriyie Mensah [a], Lin Jiang [a,*], Qiang Xu [a], Filippo Berto [c]

[a] School of Mechanical Engineering, Nanjing University of Science and Technology, Nanjing, 210094, China
[b] Structural and Fire Engineering Division, Department of Civil, Environmental and Natural Resources Engineering, Luleå University of Technology, Luleå, 97187, Sweden
[c] Department of Mechanical Engineering, Norwegian University of Science and Technology, Trondheim, 7491, Norway

ARTICLE INFO

Keywords:
Charring material
Finite element method
Surface ablation
Density variation
External heat flux

ABSTRACT

Surface ablation and in-depth temperature distribution of the charring material are the key properties of the thermal protection system in re-entry vehicles subjected to aerodynamic heating. To investigate the factors affecting the ablation performance of charring materials, the influence of decomposition reaction and surface recession on ablation was added to the heat conduction and surface energy balance equation, to comprehend the phenomenon of surface material removal. The model developed in this study was verified by comparing with results from traditional finite difference method. Furthermore, the effects of external constant heat flux, initial material thickness, and heating time on ablation were determined and discussed on temperature, surface recession, and density distribution. The change trend of the external heat flux significantly affects the change trend of the surface temperature. The material thickness and heating time have great influence on the bottom temperature. This paper contributes to the understanding of the heat transfer and ablation of the charring materials, thereby providing a basis for the selection of the thermal protection material for re-entry vehicles.

1. Introduction

For typical low earth orbit re-entry vehicle, the maximum speed and the surface temperature can reach Mach 25 and 3000 K, respectively [1]. In order for the vehicle to withstand such extreme high temperature, it is necessary to select appropriate thermal protection materials to be bonded to the airframe of the hypersonic vehicle or the blunt body of the spacecraft to provide thermal protection [2]. Thermal protection materials can effectively reduce or avoid damage to vehicle structural components caused by extremely high aerodynamic heating during hypersonic flight. On the one hand, the thermal protection material can avoid direct contact between the external heat flux and the airframe or the blunt body, while on the other hand, it consumes heat due to the decomposition reaction within the material and surface ablation. In addition, the pyrolysis gas generated by the decomposition of the resin will also act as the thermal blockage, thereby hindering the heat transfer to vehicles [3–5]. AVCOAT 5026-39H/CG, an epoxy novolac resin with special additives in a fiberglass honeycomb, is often used as the thermal protection material [6].

Charring ablation is the result of surface chemical reaction that gradually consumes the char layer of the ablative material where

* Corresponding author.
E-mail address: ljiang@njust.edu.cn (L. Jiang).

https://doi.org/10.1016/j.csite.2020.100814
Received 12 October 2020; Received in revised form 7 December 2020; Accepted 11 December 2020
Available online 15 December 2020

Nomenclature

A	pre-exponential factor, s^{-1}
C_p	specific heat, J kg^{-1} K^{-1}
E	activation energy, kJ mol^{-1}
h	enthalpy, J kg^{-1}
$\overline{h}$	mass weighted average of the material enthalpy, J kg^{-1}
k	thermal conductivity, W m^{-1} k^{-1}
L	thickness, m
$\dot{m}_g^{''}$	pyrolysis gas mass flux, kg m^{-2} s^{-1}
n	reaction order
P	pressure, Pa
q	heat flux, W m^{-2}
$\dot{s}$	surface recession rate, mm s^{-1}
T	temperature, K
t	time, s
x	coordinate, m

Greek symbols

ρ	density, kg m^{-3}
δ	volume fraction
λ	thermal blockage coefficient
σ	Stefan-Boltzmann constant, W m^{-2} K^{-4}
ε	emissivity
$\dot{\omega}$	reaction rate, s^{-1}
ϕ	porosity
ν	velocity vector, m s^{-1}
κ	permeability, m^2
μ	dynamic viscosity, Pa s

Superscripts and Subscripts

0	initial
a	surface ablation
bp	interface between the virgin layer and the pyrolysis layer
c	char layer
cold	cold wall
com	combustion
cp	interface between the pyrolysis layer and the char layer
g	pyrolysis gas
p	pyrolysis layer
r	recovery
s	surface
v	virgin layer

the char layer is formed after the material is completely decomposed at high temperature. The energy balance of the material surface is due to the complex convective and radiative heat exchange between the external flow and the material, as well as the release of pyrolysis gas and surface ablation [7]. The surface energy balance and the heat conduction equations form the basic mathematical model of the charring ablation problem. Extensive research has been done on thermal ablation of charring materials. Numerical tools like CMA [8], FIAT [9], TITAN [10], 3dFIAT [11] have been widely used. A common feature of them is that they are all based on finite difference or finite volume methods. For instance, based on central difference method, Li et al. [6] established a one-dimensional pyrolysis layer model to analyze the thermal behavior of the composite material AVCOAT. There is also a study on the thermal behavior of homogeneous and non-homogeneous charring composites during aerodynamic heating by developing a nonlinear pyrolysis layer model by central difference method [12]. Furthermore, Li et al. [13–15] developed the thermal/fluid/chemical coupling model by central difference and upwind numerical mechanism to analyze the effects of activation energy, frequency factor, composition of pyrolysis gas, and diameter of single carbon fiber on surface ablation as well as the effects of six different pore structures on ablation. Lachaud et al. [16] presented a chemical equilibrium heat and mass transport model for porous ablator by volume-averaged finite volume method. It was then applied to analyze the boundary layer and pyrolysis gas flows within the porous carbon/phenolic ablator.

Surface ablation and decomposition have been extensively investigated. For example, Park et al. [17] used the three-reaction

formula to describe the chemical reaction of the charring ablator. Curry et al. [7] combined the theoretical predictions of the ablator thermal performance obtained from the analytical model with measured data to evaluate the thermal protection performance of Apollo under both earth-orbital and lunar-return entry speed conditions and to obtain different recession rates by different controlling mechanisms. Lattimer et al. [18] expressed the decomposition reaction of charring material at high temperature by Arrhenius law and heat conduction governing equation, and obtain the thermal performance and temperature distribution. However, these methods largely depend on the heating rate, which are different from the actual conditions experienced by aerodynamic heating. Moreover, the removal of surface material due to ablation was not considered. In order to investigate the surface recession of the charring ablator, Li et al. [19] established a pyrolysis interface model, which could consider surface recession and internal pyrolysis, as well as studied the effect of different density distribution on ablation. However, the model did not consider the density change and the mass flux of pyrolysis gas between the char layer and the virgin layer. Therefore, Li et al. [12,20] developed a one-dimensional pyrolysis layer model to analyze the effect of pyrolysis between the char layer and the virgin layer on ablation. It was found that not only heat flux, moving interfaces, moving boundary, and temperature-dependent thermal properties affect the thermal behavior of the charring material but also the changing density affects the ablation. The pyrolysis layer plays a very important role in the thermal protection performance.

In this paper, a charring ablation model was established using the finite element method and the material decomposition and surface material removal were considered in the heat conduction governing equation. The decomposition reaction was expressed by Arrhenius law, which leads to the density distribution. The surface recession rate of AVCOAT 5026-39H/CG based on the reaction rate control mechanism was used to represent the surface ablation. For verification, the developed model was compared with the results of nonlinear analysis on thermal behavior using the finite difference method. Finally, the effects of external constant heat flux, material thickness, and heating time on ablation were investigated. The mathematical model consists of four parts, namely, the virgin layer, the pyrolysis layer, the char layer, and the ablation layer. In the virgin layer, the temperature may be elevated without the onset of material decomposition. The pyrolysis layer is where the composite material begins to decompose from solid into pyrolysis gas and char. The remaining material is the char or fiber matrix after the decomposition has completed. The char will oxidize leaving only a fiber matrix [18]. Experimental and theoretical studies have found that the thermal properties of charring materials change with the pyrolysis process [21–23].

2. Mathematical model

AVCOAT 5026-39H/CG, a charring material typically used in the thermal protection system, was used in this paper. During re-entry, the surface temperature of the ablative material increases and when it reaches the onset temperature T_{bp}, the resin within the material starts to pyrolyze, then the pyrolysis gas flows through the pores of the char to the ablation surface and contributes to the surface energy balance. In addition, during pyrolysis gas injection into the boundary layer, the thermal blocking effect effectively reduces the aerodynamic heating. Then the temperature continues to rise to the char formation temperature T_{cp} resulting in the generation of the char layer. When the temperature rises to the ablation temperature T_a, the surface ablation occurs, leading to the removal of surface material.

Since the temperature gradient vertically to the surface is much larger than those in other directions [24,25], a one-dimensional charring ablation model was established in this paper, as illustrated in Fig. 1, which mainly studies the heat and mass transfer, as well as the ablation characteristics.

As shown in Fig. 1, the charring material is heated by aerodynamic heating. From bottom to surface, it can be divided into four layers, which are the virgin layer, the pyrolysis layer, the char layer, and the ablation layer. L_0 is the initial thickness. The characteristics of each layer during ablation can be found in literatures [6,7,26,27]. To simplify the calculation, the following two assumptions are used:

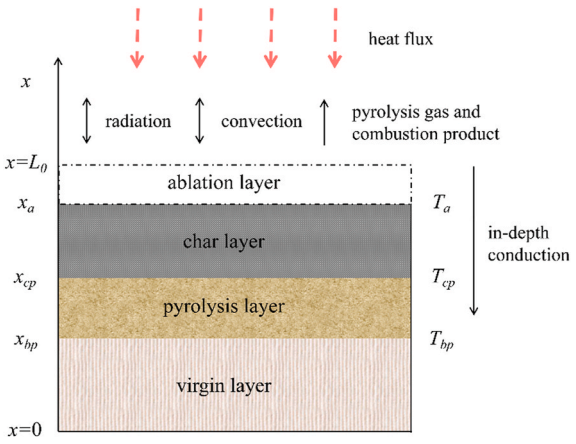

Fig. 1. One-dimensional ablation model for charring materials under aerodynamic heating.

1. When the pyrolysis gas flows through the pore structure of the char layer, there is no chemical reaction occurring between the pyrolysis gas and the porous char.
2. There is no secondary cracking of the pyrolysis gas.

The in-depth heat conduction equation that considers both the decomposition of material and removal of surface material for the one-dimensional ablation problem [18,27,28] is expressed as:

$$\rho C_p \frac{\partial T}{\partial t} = \frac{\partial}{\partial x}\left(k\frac{\partial T}{\partial x}\right) + \left(h_g - \overline{h}\right)\frac{\partial \rho}{\partial t} + \dot{m}_g^{''}\frac{\partial h_g}{\partial x} + \dot{s}\rho C_p \frac{\partial T}{\partial x}, \tag{1}$$

where ρ, C_p, and k are the density, specific heat, and thermal conductivity of the charring material, respectively, h_g is the enthalpy of pyrolysis gas, $\overline{h}$ is the mass weighted average of the material enthalpy, $\dot{m}_g^{''}$ is the mass flux of pyrolysis gas, $\dot{s}$ is the surface recession rate, x is the vertical coordinate, T is the temperature, and t is the time, similar heat transfer phenomena can also be applied in combustion processes [29–32,38].

The density change with time due to the decomposition of polymer matrix can be determined using Arrhenius equation [33],

$$\frac{\partial \rho}{\partial t} = -A\exp\left(-\frac{E}{RT}\right)\rho_v\left(\frac{\rho - \rho_c}{\rho_v}\right)^n, \tag{2}$$

where A, E, R, and n are the pre-exponential factor, the activation energy, the universal gas constant, and the reaction order, respectively. Subscripts v and c represent the virgin layer and the char layer, respectively.

In Eq. (1), both the specific heat and the thermal conductivity of the composite material are temperature-dependent, and temperature-dependent properties of the virgin layer and the char layer are given by Ref. [27]:

$$C_p = \delta C_{p,v} + (1-\delta)C_{p,c}, \tag{3}$$

$$k = \delta k_v + (1-\delta)k_c, \tag{4}$$

where δ is the volume fraction of the ablative material without decomposition, which is expressed as [27]:

$$\delta = \frac{\rho_v}{\rho_v - \rho_c}\left(1 - \frac{\rho_c}{\rho}\right). \tag{5}$$

In addition, the mass weighted average of enthalpy of material $\overline{h}$ can be defined as [27]:

$$\overline{h} = \frac{\rho_v h_v - \rho_c h_c}{\rho_v - \rho_c}, \tag{6}$$

where the enthalpy of virgin solid h_v and the enthalpy of solid char h_c are calculated based on the thermodynamic definition [18].

The enthalpy of pyrolysis gas can be determined by a function of temperature [18,27],

$$h_g = \int_{T_0}^{T} C_{p,g}\,dT, \tag{7}$$

where $C_{p,g}$ is a function of temperature [34]. On the basis of mass conservation, it is assumed that the mass of the solid is much larger than that of the gas within the charring material, as well as the sample volume remains constant during heating process, there is [18]:

$$\frac{\partial \dot{m}_g^{''}}{\partial x} = -\frac{\partial \rho}{\partial t}. \tag{8}$$

Assuming that the generated pyrolysis gas flows to the ablation surface and the mass flux at the bottom is 0, the mass flux of the pyrolysis gas during heating can be written as [18,27]:

$$\dot{m}_g^{''} = -\int_{x}^{L_0} \frac{\partial \rho}{\partial t}\,dx. \tag{9}$$

When Arrhenius kinetics are used to determine the decomposition with time, Eq. (9) can be used directly to determine the mass flux of pyrolysis gas within the material [18].

The decomposition of resin in the charring material generates pyrolysis gas and the virgin material becomes porous char, the continuity equation for the pyrolysis gas based on mass conservation can be written as [35]:

$$\frac{\partial}{\partial t}\left(\rho_g \phi\right) + \frac{\partial}{\partial x}\left(\rho_g \phi v\right) = \rho_0 \dot{\omega}_g, \tag{10}$$

where ϕ is the porosity, v is the velocity vector, and $\dot{\omega}_g$ is the gas reaction rate. The first term on the left is the gas mass change rate and

the second term is the gas mass outflow rate through the boundary of the ablator. In addition, according to Darcy's law of porous media, the gas velocity in the ablator can be expressed as [35]:

$$v = -\frac{\kappa}{\mu}\nabla P, \tag{11}$$

where κ is the permeability, μ is the dynamic viscosity, and P is the pressure.

In order to determine the thermal properties of the charring ablative material as well as for the model verification, the surface of the ablative material was heated by aerodynamic heating, while the bottom of the ablative material is insulated. The external heat flux into the material will have a radiative and convective component. Thus, the boundary condition for the material surface is denoted by Ref. [6]:

$$-k_c\frac{\partial T}{\partial x} = \lambda q - \sigma\varepsilon T_s^4 + \dot{m}_{com}^{''}h_{com}, \tag{12}$$

where q is the hot wall heat flux, σ is the Stefan-Boltzmann constant, ε is the surface emissivity, T_s is the surface temperature, $\dot{m}_{com}^{''}$ is the mass flux of combustion of surface carbon, h_{com} is the enthalpy of combustion of surface carbon, and λ is the thermal blockage coefficient, which can be given by Ref. [6]:

$$\lambda = 1 - 0.58\left(\dot{m}_{gc}^{''} + \dot{m}_{com}^{''}\right)\frac{h_r}{q_{cold}}, \tag{13}$$

where $\dot{m}_{gc}^{''}$ is the mass flux of pyrolysis gas of the char layer, q_{cold} is the cold wall heat flux, h_r is the recovery enthalpy, which can be expressed as [6]:

$$h_r = 3\times10^{-5}q_{cold}^2 - 146q_{cold} + 2\times10^8. \tag{14}$$

In addition, the hot wall heat flux q is written as [36]:

$$q = q_{cold}\left(1 - \frac{h_s}{h_r}\right), \tag{15}$$

where h_s is the wall enthalpy, which is a function of surface temperature [6].

On the basis of mass conservation [37],

$$\frac{\partial\rho_p}{\partial t} = -\frac{d\dot{m}_{gp}^{''}}{dx}, \tag{16}$$

where subscript p represents the pyrolysis layer, $\dot{m}_{gp}^{''}$ is the mass flux of pyrolysis gas of the pyrolysis layer. Assuming that the mass flux of pyrolysis gas flowing from the pyrolysis layer to the char layer is constant at $x = x_{cp}$, which is [6]:

$$\dot{m}_{gc}^{''} = \dot{m}_{gp}^{''}|_{x=x_{cp}}. \tag{17}$$

The mass flux of combustion of surface carbon can be expressed as [6]:

$$\dot{m}_{com}^{''} = \rho_c\frac{\Delta x}{\Delta t} = \rho_c\cdot\dot{s} \tag{18}$$

For the bottom of the charring ablative material [6],

$$-k_v\frac{\partial T}{\partial x} = 0. \tag{19}$$

In addition, two moving interfaces are determined by the temperature within the ablator, which are [6]:

$$T = T_{bp}x = x_{bp}, \tag{20}$$

$$T = T_{cp}x = x_{cp}. \tag{21}$$

The cold wall heat flux adopts the aerodynamic heating condition experienced by Apollo 4 during lunar-return entry [7]. During the aerodynamic heating, the density of the charring ablator changes with time, and the thermal conductivity also changes stepwise. Therefore, it is assumed that the following relationship should be satisfied on the two moving interfaces [6],

$$-k_v\frac{\partial T}{\partial x} = -k_p\frac{\partial T}{\partial x}x = x_{bp}, \tag{22}$$

$$-k_p\frac{\partial T}{\partial x} = -k_c\frac{\partial T}{\partial x}x = x_{cp}. \tag{23}$$

Assuming there is no mass exchange and gas flow at bottom boundary, which is [35]:

$$\rho_v \cdot \left(-\frac{\kappa}{\mu}\nabla P\right) = 0. \tag{24}$$

The initial conditions are defined as:

$$T_0 = 300\ \mathrm{K}, \rho_0 = \rho_v. \tag{25}$$

When the surface temperature of the ablative material reaches the ablation temperature T_a, surface ablation will occur and result in recession. In this paper, the grid moving speed is used to study the change of the physical field when the material geometry changes with the thermal parameters. During the ablation process, the linear ablation rate of the ablative material is constantly changing, which does not allow the surface to recede uniformly with time. The characterization of the linear ablation rate is usually done by dividing the ablated surface recession by the ablation time to get the average linear ablation rate, but this is not the true process of surface recession during the ablation process. In this paper, the surface recession is expressed using the surface recession rate of the ablative material AVCOAT 5026-39H/CG based on the reaction-rate-control regime, which was obtained by fitting reasonable ground test data [7]. Combining the relationship of surface recession rate with temperature and governing equations, the mass loss at each time point can be obtained. The mass loss rate is related to the surface temperature and affects the temperature distribution within the material, which significantly impacts the displacement of the moving interfaces and boundary. The initial size of the ablation sample was 0.0394 m, which is the same as the sample size in Ref. 6. An average grid size of 4e-4 m was found to produce grid independent results and has been used in all the simulations for saving calculation time. The time step of simulations is set as 0.1 s for output of results. The calculation time is 600 s, which is slightly longer than the heat flux action time.

Some property parameters such as density of the virgin layer and the char layer, thermal conductivity of the virgin layer, and emissivity of the ablation surface are constant, as shown in Table 1. In addition, there are some property parameters that are temperature-dependent [6,7,34].

3. Model validation

The comparison of surface temperature calculated by finite element method and finite difference method is shown in Fig. 2. The surface temperature calculated by finite element method is higher at each time point especially at two peaks and between 186 and 339 s. At the first peak 78 s, the surface temperature obtained by finite element and finite difference methods are 2865 and 2753 K, respectively. From 0 to 78 s, the rapid rise in temperature curves is caused by the sharp increase in external heat flux. There is a difference between two curves between 12 and 37 s, which is due to the sharp increase in thickness of the pyrolysis layer and the formation of the char layer. Furthermore, the grid size is extremely fine and the relative tolerance is small in this paper, which make the result more accurate. Then the curves drop rapidly from 78 to 186 s, which reach 1609 and 1469 K, respectively. Subsequently, the curves remain almost unchangeable until 339 s. After that, as the external heat flux increases, the temperature curves rise again to the second peaks, which are 2033 and 1927 K at 422 s. In the following heating time, the curves drop to 1123 and 1033 K at 550 s, respectively. The surface temperature calculated by finite element method is higher at each time point, because of the different values of enthalpy of pyrolysis gas. In this paper, the enthalpy of pyrolysis gas was selected as a function of temperature, which can be found in Eq. (7). As shown in Fig. 3, the enthalpy of pyrolysis gas selected in this paper is always less than the fixed value of 8.77×10^4 kJ kg^{-1}, which is the value used in finite difference method. Therefore, the heat convection by pyrolysis gas and heat absorption by decomposition of virgin material are less, thus the surface temperature at each time point is higher. In addition, it can be found that surface temperature curves have similar trend with external heat flux. External heat flux affects surface temperature, which will be discussed in the next section.

Table 1
Constant property parameters of the charring ablative material.

Parameters	Description	Data	Source
ρ_v	Density of the virgin layer	512.59 kg m-3	Refs. [6,34]
ρ_c	Density of the char layer	320.37 kg m-3	Refs. [6,34]
Kv	Thermal conductivity of the virgin layer	0.242 W m-1 K-1	Refs. [6,34]
ε	Emissivity	0.65	Refs. [6,34]
T0	Initial temperature	300 K	Ref. [6]
Tbp	Onset temperature	589 K	Ref. [6]
Tcp	Char formation temperature	811 K	Ref. [6]
Ta	Ablation temperature	1242 K	Ref. [6]
A	Pre-exponential factor	72780.37 s-1	Ref. [34]
E	Activation energy	100.69 kJ mol-1	Ref. [34]
N	Reaction order	2.5	Ref. [34]

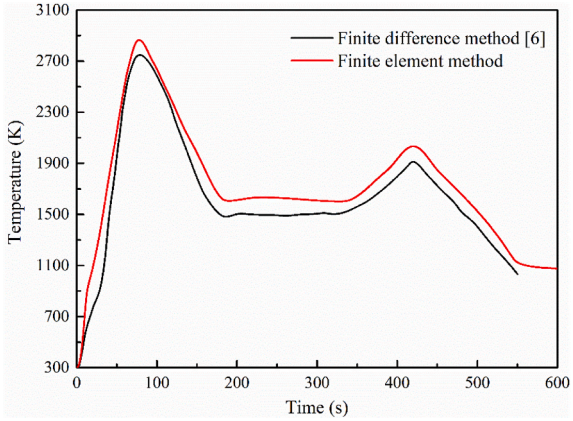

Fig. 2. Comparison of surface temperature calculated by finite difference method and finite element method.

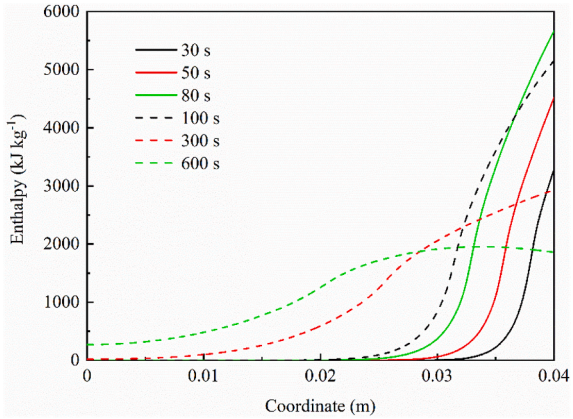

Fig. 3. Enthalpy of pyrolysis gas.

4. Results and discussion

4.1. *Effect of constant external heat flux on ablation*

According to the model validation in Section 3, it can be found that the surface temperature curve has similar trend to the external heat flux curve, the effect of constant external heat flux on ablation was discussed here.

The thermal blocking effect of pyrolysis gas and its thermal response mechanism are the main thermal protection methods of charring materials, and the study of internal temperature distribution is helpful for the analysis of the thermal protection mechanism of charring materials. Fig. 4 shows the in-depth temperature distribution history at external heat fluxes of 0.5, 1.0, 1.5, 2.0, 2.5 and 3.0 MW m^{-2}. The initial thickness of the charring ablation material before heating is 40 mm, the missing area in the figure represents the ablation thickness, which increases progressively as the external heat flux increases. When the external heat flux is 0.5 and 3.0 MW m^{-2}, the ablation thickness is 1.1 and 15.7 mm at 600 s, respectively. From Fig. 4, it can be known that the main factors influencing the ablation thickness are the external heat flux and the heating time. The pyrolysis layer is represented by the white area, which is located closer to the bottom as the external heat flux increases. The depth of heat transfer gradually increases with the increase of external heat flux. The magnitude of external heat flux considerably affects the ablation of thermal protection material, which in turn impacts the internal structural components of the aircraft. When the external heat flux is constant, the thermal protection performance of the charring material can be improved by changing the material thickness.

The surface temperature history of the ablative material under six different external constant heat fluxes also can be found in Fig. 4. It can be seen that with the increase of the heat flux, the corresponding surface temperature at each time point also increases, because with the inflow of the heat flux, the charring material absorbs heat due to its own heat capacity, which causes the surface temperature to increase. When HF = 3.0 MW m^{-2}, it reaches 2897 K at 600 s. In addition, the surface temperature reaches 1781 K at 600 s when HF = 0.5 MW m^{-2}. The surface temperature at the heat flux of 0.5 and 3.0 MW m^{-2} differs by 38.5% at 600 s. It shows that the external heat flux has a significant influence on surface temperature during ablation. The bottom temperature at each time point increases with the increase of the constant heat flux. Due to the thermal conductivity of the charring ablator, heat can be transferred to the bottom of

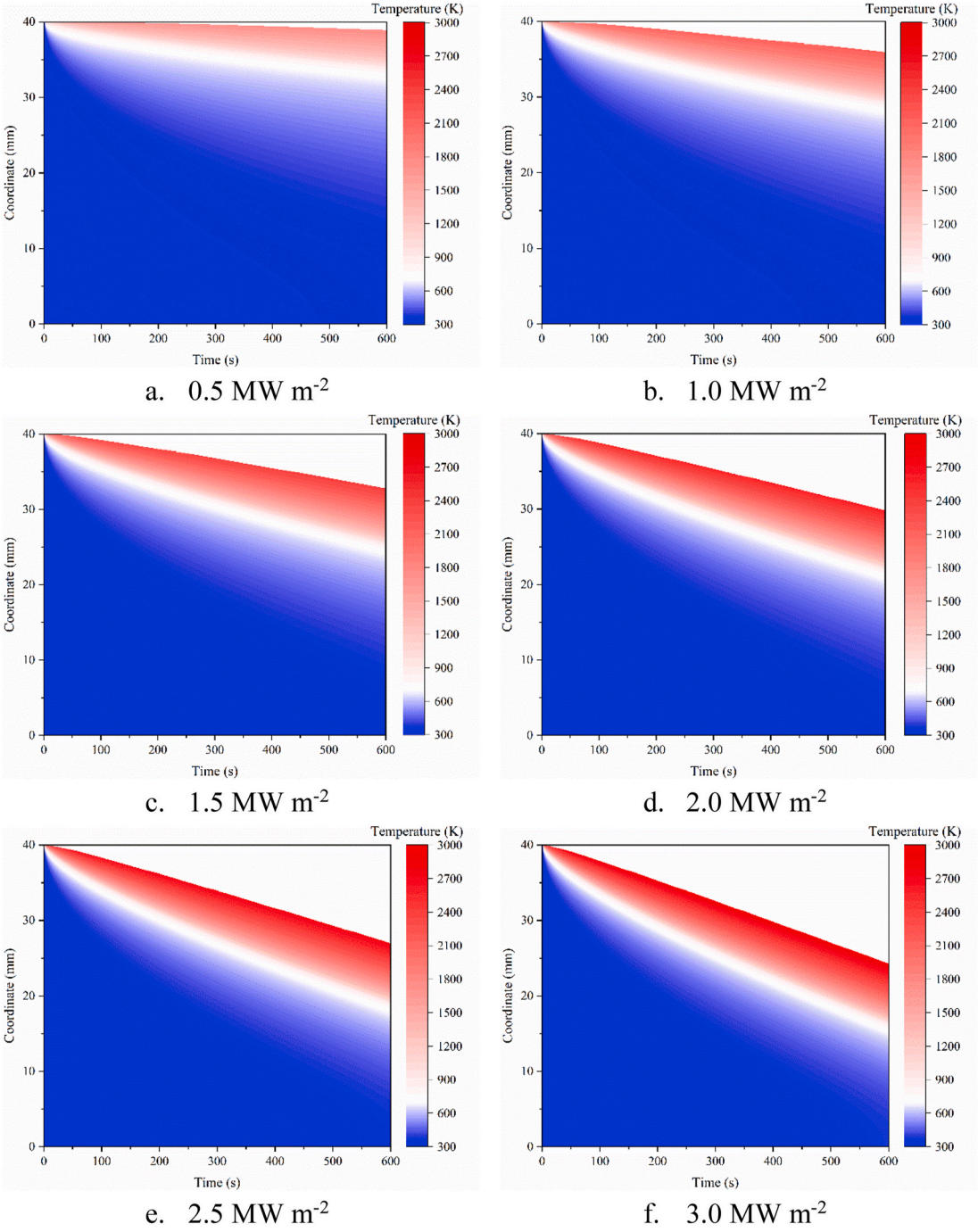

Fig. 4. In-depth temperature distribution of the ablative material at six different external heat fluxes.

the ablator, resulting in an increase in the bottom temperature. When HF = 3.0 MW m^{-2}, the temperature remains unchanged at 300 K within 200 s. This is because the heat transferred to the interior of the material was consumed by decomposition reaction of the resin, heat convection of pyrolysis gas, and surface ablation, thus heat from external aerodynamic heating has not been transferred to the bottom. With the increase of the heating time, the temperature increases gradually after 200 s, which reaches 379 K at 600 s. Therefore, not only does the external heat flux affect the ablation characteristics but also the heating time. In addition, the temperature reaches 326 K when HF = 0.5 MW m^{-2}.

Surface recession rate history of the ablative material with heating time 600 s under six different external constant heat fluxes is shown in Fig. 5. The surface recession rate at each time point increases with the increase of external heat flux. The surface temperature

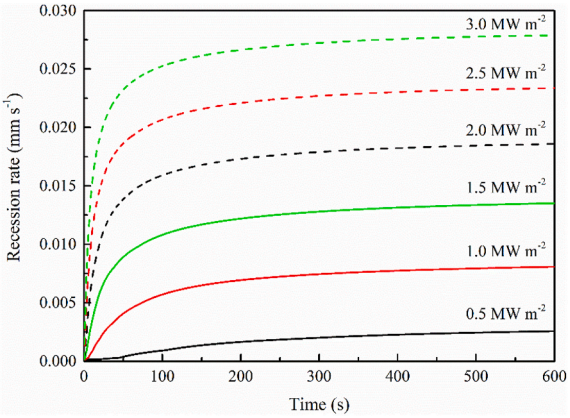

Fig. 5. Surface recession rate of the ablative material with heating time 600 s under six different external constant heat fluxes.

has a significant influence on the surface recession rate. The surface recession rate is 0 before 13 s when HF = 0.5 MW m^{-2}, which is due to the surface temperature did not yet reach the ablation temperature T_a. Subsequently, it increases slowly and reaches 0.0026 mm s^{-1} at 600 s. In addition, the surface recession rate rises sharply to 0.0216 mm s^{-1} within the first 33 s when HF = 3.0 MW m^{-2}, then it slowly increases to 0.0279 mm s^{-1} at 600 s.

The density distribution history at heating time 600 s under six different external heat fluxes can be observed in Fig. 6. It can be seen from the figure that the variation range of density increases with the increase of the external heat flux. The larger the external heat flux and the higher the temperature at the same position within the material, the faster the density changes with time. Furthermore, the depth of heat transfer is also larger when the heating time is same, thus the density variation range is larger. The density keeps constant at 512.59 kg m^{-3} between 0 and 12.5 mm when HF = 3.0 MW m^{-2}, then it suddenly drops from 12.5 to 23.2 mm due to the decomposition of the resin. Finally it remains unchanged at 320.37 kg m^{-3}.

4.2. *Effect of material thickness on ablation*

The effect of the material thickness on ablation was discussed in this section and the external heat flux is set as 1.5 MW m^{-2}. The bottom temperature history for five different material thicknesses is shown in Fig. 7. It can be seen that as the thickness of the material decreases, the influence on the bottom temperature increases. Moreover, the corresponding temperature at each time point increases with the thickness decreasing. Decreasing the initial thickness of the material results in less heat consumption due to heat conduction, more heat being transferred to the bottom, resulting in greater influence on bottom temperature. When the thickness is 0.02 m, the temperature does not change in the first 63 s, indicating that the heat has not been transferred to the bottom. Subsequently, the temperature curve has a large gradient and reaches 615 K at 600 s. When the thickness is 0.06 m, there is almost no change in bottom temperature, which is 301 K at 600 s. It can be seen that by appropriately increasing the thickness the bottom temperature can be reduced effectively, thereby protecting the internal structural parts of the aircraft.

Fig. 8 shows the surface recession rate with heating time 600 s for five different material thicknesses. The thickness of the charring material has little effect on surface recession rate, just like surface temperature. The surface recession rate increases significantly from

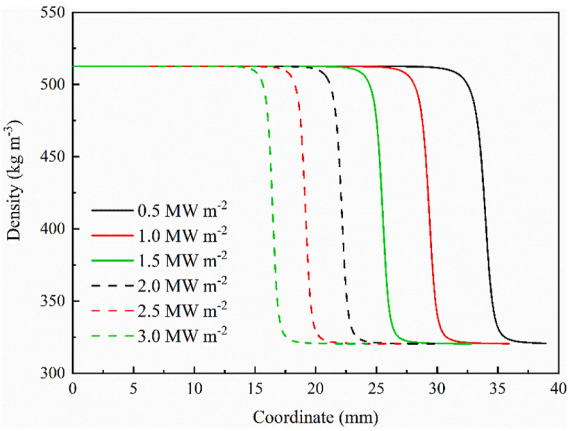

Fig. 6. Density distribution of the ablative material at heating time 600 s under six different external constant heat fluxes.

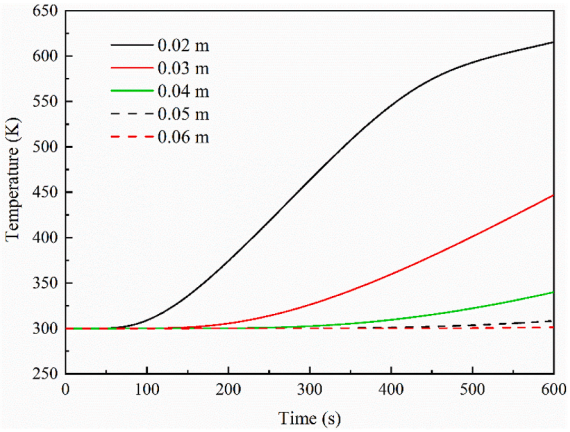

Fig. 7. Bottom temperature of the ablative material with heating time 600 s for five different material thicknesses.

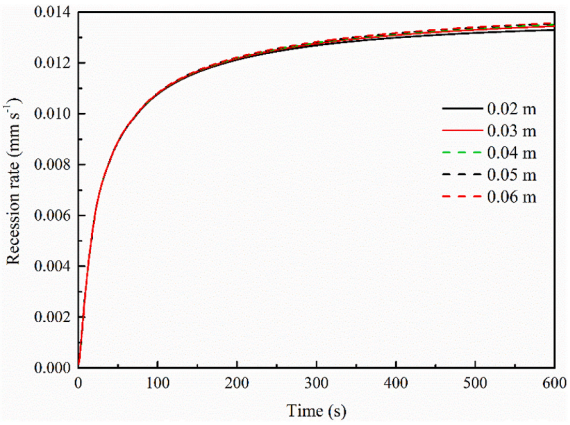

Fig. 8. Surface recession rate of the ablative material with heating time 600 s for five different material thicknesses.

0 to 0.0096 mm s^{-1} during the first 63 s, then its gradient decreases and "steady ablation" occurs. Finally, it reaches 0.0136 mm s^{-1} at 600 s.

4.3. Effect of heating time on ablation

According to Fig. 4, the ablation thickness increases with the increase of the heating time when the external heat flux is constant, thus the heating time also affects ablation to some extent. This section mainly investigates the effect of heating time on ablation.

Fig. 9 illustrates the in-depth temperature distribution within the ablative material for different heating times. As the heating time increases, the temperature at the same coordinate also increases. The missing area represents the thickness that has been ablated. The ablation thickness increases with the increase of the heating time. When heating times is 400 and 1400 s, the ablation thicknesses are 4.5 and 18.2 mm, respectively. The white area indicates the pyrolysis layer, where the temperature range is from T_{bp} to T_{cp}. Furthermore, the position of the pyrolysis layer is closer to the bottom of the ablative material as the heating time increases, indicating a greater the depth of heat transfer. Therefore, the heating time significantly affects the temperature distribution of the charring material. Excessive heating time may affect the operation of the aircrafts.

From Fig. 9, the surface temperature for different heating times can be known. The complex convective and radiative heat exchange for the material surface lead to the surface energy balance. With heating times of 400 and 1400 s, the surface temperature eventually reach 2401 and 2436 K, respectively. The heating time affects the surface temperature to a certain extent but the most important factor is the external heat flux.

5. Conclusions

In this paper, in order to study the factors affecting the ablation performance of charring materials, a one-dimensional charring ablation model was developed by finite element method. By comparing with the results of nonlinear analysis for the charring material using the finite difference method, it was found that there are some differences between two methods. Since the enthalpy of pyrolysis

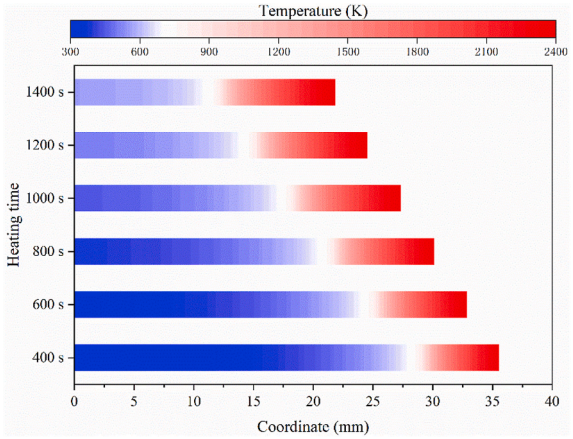

Fig. 9. In-depth temperature distribution within the ablative material at different heating times.

gas in this investigation is a function of temperature rather than a constant value and it is always less than that constant value, the heat convection by pyrolysis gas and the decomposition of virgin material result in less heat consumption. However, in general the model can be used for ablation analysis of the charring material. Subsequently, the effects of external heat flux, initial material thickness, and heating time on ablation were discussed. The external heat flux significantly affects the surface temperature, as well as the surface recession rate. The greater the initial thickness, the lower the bottom temperature for the same heating time. Heating time affects the ablation thickness and in-depth temperature distribution. The one-dimensional model also has two shortcomings. Firstly, the model does not consider the effects of complex geometries on ablation. Secondly, the relationship between the surface recession rate and the temperature is fixed resulting in large influence of surface temperature on surface recession rate, while the influence of other factors on surface recession rate is poorly considered.

Author statement

Jie Xiao: Writing – original draft, Writing – review, Methodology, Model verification, Numerical simulation.
Oisik Das: Writing – review & editing, Supervision.
Rhoda Afriyie Mensah: Writing – review & editing.
Lin Jiang: Writing – review & editing, Supervision, Verification, project administration, Numerical simulation.
Qiang Xu: Writing – review & editing, Supervision.
Filippo Berto: Methodology.

Declaration of competing interest

The authors declare that they have no known competing financial interests or personal relationships that could have appeared to influence the work reported in this paper.

Acknowledgment

The authors would like to thank National Natural Science Foundation of China (NSFC, Grant 51806208).

References

[1] J.D. Anderson, Hypersonic and high temperature gas dynamics, AIAA (2000).
[2] M. Natali, J.M. Kenny, L. Torre, Science and technology of polymeric ablative materials for thermal protection systems and propulsion devices: a review, Prog. Mater. Sci. 84 (2016) 192–275.
[3] T. Suzuki, T. Sakai, T. Yamada, Calculation of thermal response of ablator under arcjet flow condition, J. Thermophys. Heat Tran. 21 (2007) 257–266.
[4] H. Huang, W. Li, C. Xu, X. Xu, The inverse problem in zero linear ablation of aluminizing carbon composites under high heat flux, Therm. Sci. 17 (2013) 1323–1327.
[5] H.M. Huang, W.J. Li, H.L. Yu, Thermal analysis of charring materials based on pyrolysis interface model, Therm. Sci. 18 (2014) 1591–1596.
[6] W. Li, H. Huang, Y. Tian, Z. Zhao, Nonlinear analysis on thermal behavior of charring materials with surface ablation, Int. J. Heat Mass Tran. 84 (2015) 245–252.
[7] D.M. Curry, E.W. Stephens, Apollo ablator thermal performance at superorbital entry velocities, Nat Aeronaut. Space Administration (1970).
[8] R.M. Kendall, R.A. Rindal, E.P. Bartlett, A multicomponent boundary layer chemically coupled to an ablating surface, AIAA J. 5 (1967) 1063–1071.
[9] Y.K. Chen, F.S. Milos, Ablation and thermal response program for spacecraft heatshield analysis, J. Spacecraft Rockets 36 (1999) 475–483.
[10] Y.K. Chen, F.S. Milos, Two-dimensional implicit thermal response and ablation program for charring materials, J. Spacecraft Rockets 38 (2001) 473–481.
[11] Y.K. Chen, F.S. Milos, Multidimensional finite volume fully implicit ablation and thermal response code, J. Spacecraft Rockets 55 (2018) 914–927.
[12] W. Li, H. Huang, B. Ai, Z. Zhang, On the novel designs of charring composites for thermal protection application in reentry vehicles, Appl. Therm. Eng. 93 (2016) 849–855.

[13] W. Li, H. Huang, X. Xu, J. Guo, A new mechanism of surface ablation of charring materials for a vehicle during reentry, Appl. Therm. Eng. 106 (2016) 838–849.
[14] W. Li, J. Liang, J. Ge, Novel designs of charring composites based on pore structure control and evaluation of their thermal protection performance, Int. J. Heat Mass Tran. 129 (2019) 59–73.
[15] W. Li, J. Ge, J. Liang, Influence factors on the multi-field coupling performances of charring ablators on the basis of a mesoscopic ablation model, Appl. Therm. Eng. 161 (2019) 114–126.
[16] J. Lachaud, T. van Eekelen, J.B. Scoggins, T.E. Magin, N.N. Mansour, Detailed chemical equilibrium model for porous ablative materials, Int. J. Heat Mass Tran. 90 (2015) 1034–1045.
[17] C. Park, R.L. Jaffe, H. Partridge, Chemical-kinetic parameters of hyperbolic earth entry, J. Thermophys. Heat Tran. 15 (2001) 76–90.
[18] B.Y. Lattimer, J. Ouellette, J. Trelles, Thermal response of composite materials to elevated temperatures, Fire Technol. 47 (2009) 823–850.
[19] W. Li, H. Huang, Z. Zhang, X. Xu, Effects of gradient density on thermal protection performance of AVCOAT composites under varied heat flux, Polym. Compos. 37 (2016) 1034–1041.
[20] W. Li, H. Huang, X. Xu, Z. Zhao, Nonlinear pyrolysis layer model for thermal behavior of nonhomogeneous charring materials, J. Appl. Polym. Sci. 132 (2015) 42331.
[21] A.P. Mouritz, S. Feih, E. Kandare, Z. Mathys, A.G. Gibson, P.E. Des Jardin, S.W. Case, B.Y. Lattimer, Review of fire structural modelling of polymer composites, Compos. Part A-Appl. S. 40 (2009) 1800–1814.
[22] F. Milos, C. Scott, S. Del Papa, Arcjet testing and thermal model development for multilayer felt reusable surface insulation, J. Spacecraft Rockets 51 (2) (2014) 397–411.
[23] J.M. Park, D.J. Kwon, Z.J. Wang, J.U. Roh, W.I. Lee, J.K. Park, K. Lawrence DeVries, Effects of carbon nanotubes and carbon fiber reinforcements on thermal conductivity and ablation properties of carbon/phenolic composites, Compos. Part B-Eng. 67 (2014) 22–29.
[24] H. Belghazi, M. El Ganaoui, J.C. Labbe, Analytical solution of unsteady heat conduction in a two-layered material in imperfect contact subjected to a moving heat source, Int. J. Therm. Sci. 49 (2010) 311–318.
[25] H. Huang, X. Xiaoliang, G. Huang, Z. Zhang, Thermal response of heat-resistant layer with pyrolysis, Therm. Sci. 16 (2012) 69–78.
[26] T.K. Risch, Verification of a finite element model for pyrolyzing ablative materials, in: 47th AIAA Thermophysics Conference, Denver, USA, 2017, p. 3354.
[27] Y. Wang, T.K. Risch, J.H. Koo, Assessment of a one-dimensional finite element charring ablation material response model for phenolic-impregnated carbon ablator, Aero. Sci. Technol. 91 (2019) 301–309.
[28] Y. Wang, T.K. Risch, C.L. Pasiliao, Modeling of pyrolyzing ablation problem with ABAQUS: a one-dimensional test case, J. Thermophys. Heat Tran. 32 (2018) 544–548.
[29] Kaiyuan Li, Simo Hostikka, Dai Peng, Yuanzhou Li, Heping Zhang, Jie Ji, Charring shrinkage and cracking of fir during pyrolysis in an inert atmosphere and at different ambient pressures, Proc. Combust. Inst. 36 (2017) 3185–3194.
[30] Huaxian Wan, Z. Gao, Jie Ji, Liangzhu Wang, Yongming Zhang, Experimental study on merging behaviors of two identical buoyant diffusion flames under an unconfined ceiling with varying heights, Proc. Combust. Inst. 37 (2019) 3899–3907.
[31] Zihe Gao, Jie Ji, Huaxian Wan, Jinhua Sun, An investigation of the detailed flame shape and flame length under the ceiling of a channel, Proc. Combust. Inst. 35 (2015) 2657–2664.
[32] Yujia Sun, Shu Zheng, Influence of particle rotation and partial irradiation on the particle heating up process, Int. Commun. Heat Mass 119 (2020) 104892.
[33] Y. Wang, Multiphysics analysis of lightning strike damage in laminated carbon/glass fiber reinforced polymer matrix composite materials: a review of problem formulation and computational modeling, Compos. Part A-Appl. S. 101 (2017) 543–553.
[34] S.D. Williams, D.M. Curry, Thermal Protection Materials: Thermophysical Property Data, NASA STI/Recon Technical Report N, 1992. Report/Patent Number: NASA-RP-1289, S-693, NAS 1.61:1289.
[35] J. Yang, H. Chen, N. Liu, Modelling of two-dimensional natural downward smoldering of peat, Energy Fuel. 30 (10) (2016) 8765–8775.
[36] M.B. Dow, R.T. Swann, S.S. Tompkins, Analysis of the effects of environmental conditions on the performance of charring ablators, J. Spacecraft Rockets 3 (1966) 61–67.
[37] A.G. Gibson, T.N.A. Browne, S. Feih, A.P. Mouritz, Modeling composite high temperature behavior and fire response under load, J. Compos. Mater. 46 (2012) 2005–2022.
[38] X.Y. Xiong, K. Gao, J. Zhang, B. Li, L.F. Xie, D. Zhang, A.M. Rhoda, Interaction between shock wave and solid particles: Establishing a model for the change of cloud's expansion rate, Powder. Technol. (2020).